Atmos. Chem. Phys. Discuss., 11, 10485–10523, 2011
www.atmos-chem-phys-discuss.net/11/10485/2011/
doi:10.5194/acpd-11-10485-2011

Atmospheric Chemistry and Physics Discussions

Study on long-term aerosol distribution over the land of East China using MODIS data

Q. He[1], C. Li[2], F. Geng[1], Y. Lei[3], Y. Li[4], X. Tie[1], and Q. Yin[1]

[1]Shanghai Meteorological Bureau, Shanghai, China
[2]Laboratory for Climate and Ocean-Atmosphere Studies, Department of Atmospheric Sciences, School of Physics, Peking University, Beijing, China
[3]Meteorological Observation Centre of CMA, Beijing, China
[4]Shanxi Meteorological Bureau, Taiyuan, China

Received: 28 February 2011 – Accepted: 23 March 2011 – Published: 4 April 2011

Correspondence to: C. Li (ccli@pku.edu.cn)

Published by Copernicus Publications on behalf of the European Geosciences Union.

Abstract

East China is among the fastest developing and most populous area in Asia, where atmospheric aerosol loading is high due to heavy urban and industrial emission. These aerosols may have significant impact on regional climate and environment. In this report, MODIS level 2 aerosol products (2000–2007) were used to study aerosol spatial and temporal distributions, as well as their variations with local meteorological conditions over East China. By combining Aerosol Optical Depth (AOD) and aerosol Fine Mode Fraction (FMF), we found that the urban/industrial aerosol and dust are two dominant species over northern part, whereas continental, marine and mixed aerosols dominate the southern part of East China, except for Poyang Lake Plain. Both annual mean AOD and area with high AOD increased from 2000 to 2007, with the largest increase seen in Yangtze River Delta region (YRD). In summer, AOD in East China reached the maximum of about 0.8 in YRD, dominated by fine mode particles. The minimum AOD occurred in winter with mostly coarse mode particles. The higher AOD in spring is attributed to coarse particles. Local aerosol properties were analyzed in three typical zones: the northern dry zone (I), the central urban/industrial zone (II) and the southern natural background zone (III). Monthly mean AODs in zone I and II were above 0.5 throughout the entire year, with the maximum AOD in June. High FMFs in this period indicated heavy urban and industrial pollutions. Monthly mean AODs and FMFs in zone III reached maximum of 0.51 in April and September (up to 90.7%) respectively. High AOD in spring in zone III appears mostly due to the long-range dust transport from the North. In fact, dust particles contributed 50–80% to aerosol loading in zone I and II, but only 20% in zone III. The effect of meteorological conditions such as temperature, relative humidity (RH) and wind on aerosol loadings over East China were also investigated.

ACPD
11, 10485–10523, 2011

1 Introduction

Aerosols are a major factor affecting Earth's radiation budget and hydrologic cycle. They affect climate through direct interactions with solar and terrestrial radiation (direct aerosol effect), and through their effect on the optical and microphysical properties and lifetime of clouds (indirect aerosol effect) (Charlson et al., 1992; Levine et al., 1995; Haywood and Boucher, 2000). Atmospheric aerosols in high concentrations can also affect human and reduce the visibility. The biggest uncertainty in climate change, even by the best available General Circulation Models, is due to uncertainties in aerosol radiative forcing (IPCC, 2001). This uncertainty arises mainly because of our poor understanding on both aerosols temporal and spatial distributions and their associated properties (Pilinis et al., 1995). In order to carry out model studies of the global climate change, global aerosol concentrations over a long time period is needed. Studies of aerosol properties at different locations are essential to our understanding of the recent climate change (IPCC, 2001).

Different techniques are available to measure spatial and temporal variations of aerosols. On a global scale, remote sensing instruments such as the Moderate Resolution Imaging Spectroradiometer (MODIS) on aboard both polar orbiting TERRA and AQUA satellites continue to produce global AOD maps retrieved from backscattered solar radiation through the atmosphere (Hutchison et al., 2005; Kaufman et al., 2003; King et al., 1992; Levy et al., 2003; Tang et al., 2005). These satellite-based remote sensing techniques offer a much wider spatial view than in-situ or surface-based radiometric observations. Satellite-retrieved AOD can be a useful parameter for the estimation of optical and physical characteristics of aerosol on the regional scale. Recently, MODIS-derived aerosol properties have enabled us to comprehensively study the spatial and temporal variations of aerosols (Barnaba and Gobbi, 2004; Chu et al., 2005).

East China is a fast developing and densely populated region in the world, and a major source of aerosol emissions where loadings are high and chemical/physical properties are complex (Li, 2004). A handful of field experiments have been conducted

ACPD
11, 10485–10523, 2011

in this region such as the Asian-Pacific Regional Aerosol Characterization Experiment (ACE-Asia) (Huebert et al., 2003) and the Asian Atmospheric Particle Environment (APEX) (Nakajima et al., 2003). Luo et al. (2001) analyzed AOD at 750 nm observed from 46 stations in China and concluded that the middle and back drainage area of YRD has been characterized by most distinct AOD increase since 1980s. Many cities in East China experienced high airborne particle concentrations emitted from biomass burning, motor vehicle exhaust, as well as secondary sulfates formed from the sulfur dioxide by atmospheric chemical reactions. Heavy aerosol loading in this region has been reported based on ground and satellite instruments. Regional temperature and precipitation pattern changes from the mid-1970s were suggested to relate to the heavy aerosol loading and aerosol's strong absorption in East China (Xu, 2001; Qian and Giorgi, 2000; Menon et al., 2002). Using data from GMS, Mao et al. (2005) found relatively higher AOD in the middle and back drainage area of YRD and coastal region in East China. Xu et al. (2002) analyzed aerosol chemical/physical and radiative data observed in Lin'an, Sheshan and Changshu city of YRD in 1999, and found that the aerosol radiative properties in Lin'an, a typical rural background, showed more urban rather than rural characteristics.

The underlay characteristics of East China is complicated with coasts, plains and mountains. The temperature, precipitation and relative humidity vary largely with different seasons, and can significantly influence the temporal and spatial distributions of aerosols. The growing population and transportation in East China has resulted in high demands on energy. Aerosol from urban/industrial emissions, dusts, and sea salt brought by wind all contribute jointly to the regional aerosol loading. Furthermore, agricultural biomass burning aerosols can also be transported into East China from the surrounding rural area in June.

In the previous studies, most of the aerosol characteristic over east China was studied using the observation data (such as sunphotometer) from discrete sites. The long-term continuous observation for the spacial and temporal distribution of aerosol from satellite was scarce. It should be noted that the complicated spacial and temporal

ACPD
11, 10485–10523, 2011

distribution caused by the rapid economic growth in this region have already reduced the accuracy of climate simulation which usually takes the climatologic meaning value of aerosol attribution as input. As a result, the climatologic meaning value was incapable to describe precisely the effect on regional climate and environment change induced by aerosol and so more detailed and high spacial and temporal resolution aerosol information is prerequisite. In this paper, we synthesize the multi-year data sets of column-integrated aerosol optical and physical properties obtained from satellite-based sensor MODIS to investigate regional aerosol characteristics over East China. We considered four seasons: spring (MAM) (dry and dusty), summer (JJA) (rainy and accounts for about two-thirds of the annual precipitation), autumn (SON) (anticyclone is a dominant system), winter (DJF) (windy, sunny and dry). Parameters used in this study include AOD at 550 nm, Angstrom exponent α and FMF. All products are given at a spatial resolution of $0.1^{\circ} \times 0.1^{\circ}$. The FMF is defined as the ratio of optical depth (550 nm) of fine-mode particles to that of fine- and coarse-mode aerosols at 550 nm based on the assumption of bi-modal lognormal size distributions.

2 MODIS aerosol algorithm and geographical and climatic characteristics

MODIS AOD retrieval over land employs primarily three spectral channels centred at 0.47, 0.66, and 2.1 µm. AOD is derived at 0.47 and 0.66 µm, and interpolated to 0.55 µm. It is only retrieved for cloud-free pixels in each 20×20 pixel area, and over surfaces that are not too bright, with a $10 \times 10\,km^2$ resolution. The reflectivity measured at 2.1 µm at the top-of-atmosphere is used to infer surface reflectivity at that wavelength. Fine-mode particles (including secondary aerosols, primary aerosols from traffic and industrial sources, and biomass burning aerosols), which dominate in the AOD in most parts of China, have a negligible optical thickness at 2.1 µm, allowing for almost direct observations of the surface (Chu et al., 2003). The surface reflectivity at visible wavelengths is then obtained by assuming a constant ratio between surface reflectivity at 2.1 µm and that at 0.47 and 0.66 µm. In reality, this ratio depends on the

ACPD
11, 10485–10523, 2011

surface type and is time-dependent (e.g., vegetation and soil moisture). In the current MODIS algorithm, this is not taken into account, and may lead to systematic biases in retrieved AOD depending on surface type and season. MODIS aerosol algorithm over land chooses a set of fine-mode dominated aerosol models and a single coarse-mode dominated aerosol model (Kaufman et al., 1997; Remer et al., 2005). The selection of fine-mode aerosol model is fixed wih the season and location. The coarse-mode dominated model (dust) is fixed globally. The retrieval algorithm had a choice of two fine modes, the "urban/industrial," and the "biomass burning/developing world," differing as to their refractive indices, single scattering albedos (SSA or ω_0), and phase functions. Each of these aerosol types is actually comprised of two or more lognormal modes (Kaufman et al., 1997), with their optical properties based on a combination of laboratory studies and Sun photometer data (Remer and Kaufman, 1998).

The fine fraction of AOD (FMF), is determined from the spectral dependence of the path radiances at 0.66 and 0.47 µm (Kaufman et al., 1997; Remer et al., 2005), which provides an indication of whether the AOD is dominated by fine mode or coarse mode aerosols. The fine mode aerosols over urban, industrialized and densely populated regions are mainly due to the gas to particle conversion (fossil fuel, biomass combustion-anthropogenic), while coarse mode aerosols such as windblown mineral dust and sea salt particles mainly arise from natural sources. Though MODIS derived FMFs have not been validated over large area on land, they provide a good indication of the type of aerosol (fine or coarse) that dominates the size distribution. Ramachandran (2007) validated and compared MODIS derived FMFs with monthly mean in situ AERONET measurements over Kanpur in north India, and found a good agreement during most of the months. The aerosol properties over East China are similar to those over north India. Therefore MODIS derived FMFs can be used to investigate the temporal/spatial distribution and classify the aerosol type in East China.

The major error sources of MODIS derived AOD are the assumed constant ratio between surface reflectivity at 2.1 µm and that at visible wavelengths. In order to improve the retrieval accuracy, the second-generation operational algorithm performs

ACPD
11, 10485–10523, 2011

a simultaneous inversion of two visible (0.47 and 0.66 μm) and one shortwave-IR (2.12 μm) channel, considers the influence of scattering angle (including solar zenith angle, viewing zenith angle), surface type and NDVI to the assumed surface reflectivity relationship. The new algorithm also replaced the assumed aerosol mode optical properties with the multi-year measurement from AERONET. Preliminary validation of this algorithm shows much improved retrievals of AOD, where the MODIS/Aerosol Robotic Network t (at 0.55 μm) correlation coefficient is up to 0.90 (Levy et al., 2007).

We used the 10 × 10 km MODIS derived AODs and FMFs to obtain the diurnal and monthly mean values over East China, and then the annual and 8-year mean values. Contributions of different aerosol types to AOD are also estimated at each pixel.

East China ranges from the mid-latitudes to the subtropical zone, with complicated topography characterized by mostly plains in the northern part, and mountains in the southern part. Figure 1 gives the location of East China with topography. Anhui Province, a territory in the northern part, has the maximum coal storage and steel industrial base. The Yangtze River, the longest river in China, traverses East China region and flows into the East China from west. Cities with more than one million in population include Shanghai (one of the largest city in the world), Nanjing, Hangzhou, Suzhou, Wuxi, Ningbo, Changzhou, Jinan, Hefei, Nanchang and Fuzhou. Most of these cities are located in the Yangtze River Delta region, whose industrial outputs account for nearly 1/4 in China.

Divided by the Yangtze River, the northern and southern parts of East China are controlled by different climate zone. The northern part is in the transition zone from warm temperate monsoon region to subtropical climate, characterized by uneven seasonal precipitation distributions. 60 ~ 70% of its annual precipitation occurs between June and August, with the Plum rain and the Autumn rain (also tropical cyclones) as the main contributors. The Plum rain, a typical weather in middle and lower reaches of the Yangtze River region, usually starts in mid-June and ends in earlier July. Monsoon changes significantly with different seasons. In winter, this region is controlled by the Mongolia high pressure and the Aleutian low pressure, and influenced by frequent

ACPD
11, 10485–10523, 2011

cold air invasion from the north. This results in the prevalence of the north-westerly and north-easterly winds with cold and dry weather. In summer, continental heat low pressure produces the prevailing south-easterly wind with warm and humid weather. The Northwest Pacific subtropical high dominants in July and August and sometimes brings hot and dry air. North-easterly and easterly winds usually prevail in spring and autumn, bringing frequent cold and wet condition and convection.

The southern part is a typical subtropical monsoon climate zone, affected by the East Asian monsoon, with seasonal changes in prevailing wind direction and precipitation amount. In spring, the northerly and southerly flows switch frequently. In summer, this region is controlled by the prevailing southeast wind and the northwest Pacific subtropical high activities. In autumn, frequent cyclones lead to abundant precipitation. In winter, the dominant northerly wind is usually companied by dry, cold weather. More than 50% of the annual precipitation occurs from April to July.

3 Results and discussion

3.1 Summary of aerosol distributions in East China

AOD and Angstrom exponent α over East China derived from MODIS are averaged from 2000 to 2007 and shown in Fig. 2. Areas in East China with high AOD are found in the densely populated and industrialized areas (individual cities and clusters of cities). Very high values are found in the northwest plain in Shandong province, Huanghuai, Poyang Lake Plain and the Yangtze River Delta region (especially in areas along the Yangtze River). Some small scale features, such as major cities (Nanjing, Shanghai) can be distinguished. Low AOD values are observed in southern part and over the mountains throughout East China (Wuyi cordillera, etc.). Clearly, most aerosols are detected being close to their source regions. As a highly urbanized area with dense population and developed industry, the Yangtze River Delta is characterized by a rich aerosol emission region. Northwestern Shandong plain has lower urbanization compared with

ACPD
11, 10485–10523, 2011

YRD, but it is vulnerable to dust transported from North China. In addition, the Yimeng cordillera on the eastern Shandong province blocks the west flow, resulting in aerosol accumulation along nearby western border of the cordillera. Aerosol distributions in Huanghuai region also strongly depend on topography and industry locations. The Yangtze River valley in Anhui Province was surrounded by Dabie and Tianmu cordillera. It has several cities with more than one million population and numerous copper smelting industry and coal bases. Aerosols emitted in this region are hard to dissipated. On the other hand, this region is one of the main channels of aerosol transport from the west. Poyang Lake plain, surrounded by the mountains, suffers severe aerosol accumulation due to the basin effect and high anthropogenic emission.

The Angstrom exponent depends on the size of the aerosol particles. It is small for coarse particles and increases with decreasing particle size. According to MODIS, the Angstrom exponent ranges from 0 to 1.8 for the most parts of East China, but appears to be lower over the northern part than the southern part. Angstrom exponent is anti-correlated with AOD, which indicates that the increasing AOD over East China is mainly caused by those aerosol particles with large size, possibly produced by constructive activities and poor vegetation cover condition in China (He et al., 2006). In East China, the smallest α values are usually located in coastal areas, which represent the sea salt particles. The largest α values (>1.6) are usually located in Tianmu cordillera in Zhejiang, Qiyun cordillera in Jiangxi and Hawksbill cordillera in Fujian, which are typically water-soluble aerosol particles. The α varies in the range between 0.6 and 1.0 in the northern part of East China and the Poyang Lake plain indicating mostly the mixed aerosols of continental and urban/industrial particles. However, caution must be note here that the α is even more sensitive to the assumptions on the spectral dependence of the land surface than the AOD, and may be biased for specific surface type or season.

ACPD
11, 10485–10523, 2011

3.2 Distribution of aerosol types

Following Barnaba and Gobbi (2004), a simple method for classifying main aerosol types from MODIS data was developed, the aerosols with AOD(550 nm) ≤ 0.3 and FMF < 0.8 are considered to be marine type, AOD(550 nm) > 0.3 and FMF < 0.7 for dust, and all the other aerosols are considered of continental type (AOD(550 nm) < 0.3 and FMF > 0.8 or AOD(550 nm) > 0.3). This classification method does not consider biomass burning and urban/industrial aerosol. Dubovik et al. (2002) investigated the aerosol optical properties obtained from sun photometers located in several typical sites and found that the averaged AODs (440 nm) of the biomass burning aerosol are 0.75 and 0.39 in Brazil and North America respectively. The industry is flourishing in Brazil, similar to East China. Therefore, aerosols with AOD(550 nm) ≥ 0.7 and FMF ≥ 0.7 in East China can be considered to be of biomass burning type, and AOD(550 nm) > 0.3 with FMF between 0.35 and 0.7 from urban/industrial emission.

Figure 3 presents aerosol type distributions in East China according to the AOD ~ FMF classification method. The dominant aerosols in the southern part of East China (excluding the Poyang Lake plain) are continental, marine and mixed types. Continental aerosol type dominated in southern Anhui and central Zhejiang. Abundant marine aerosols were found over mountain area of East China, but the dominant aerosol type over coastal zone is mixed aerosol rather than marine aerosol. This is possibly due to some small cities along the coast where human activities produce plenty of anthropogenic pollutants.

Similarly, we found that the dominant aerosols over YRD are soil dust and urban/industrial type. This is possibly connected to the windblown mineral dust storms that usually occur in the spring (Kim, 2005). Another interesting feature in Fig. 3 is that aerosols originated in North and West China are transported by the strong westerly flow and can affect aerosol loadings in downwind areas. As shown in Fig. 3, AOD decreased gradually away from the North China. The urban/industrial type dominates in YRD, the cross zone of Jiangsu, Anhui and Shandong, Poyang Lake plain, and some

ACPD
11, 10485–10523, 2011

cities along the southeastern coast, where numerous industry enterprises emitted large amount of anthropogenic pollutants. This result suggests that columnar aerosol optical properties over YRD are often influenced both by dust and anthropogenic pollutants during the entire year.

3.3 Annual variation of AOD over East China

Annual mean AOD over East China from 2000 to 2007 are presented in this section. Several significant characteristics can be found in Fig. 4.

3.3.1 Increasing trend in aerosol loading

Areas with AOD > 0.5 and AOD > 1.0 was expanding, especially after 2005. Aerosol pollution area where the AOD > 0.5 and 1.0, and its proportion to the different regions, such as YRD, Shandong, Anhui, respectively, and pollution intensity (the mean, maximum, minimum AOD and its location) in different regions were calculated from 2000 to 2007 and listed in Table 1. In year 2000, the area with annual mean AOD > 1.0 only covered a few cities along the Shanghai-Nanjing Railway. It extended to most parts of Jiangsu province and accounted for 4.3% of total area in YRD in 2007. The aerosol pollution increased rapidly after the year of 2006 and the area with AOD > 1.0 in 2007 was about 20 times of that before 2005. Moreover, the maximum annual mean AOD increased from 0.8 in 2001 to 2.4 in 2007, and the minimum annual mean AOD increased by 0.08 from 2002 to 2005 in YRD.

There were few areas with annual mean AOD > 1.0 before 2002, but the area with annual mean AOD > 0.5 spread widely even in the cleanest year of 2001 (up to 70%) in Shandong province. In the most polluted year of 2006, the area with annual mean AOD > 0.5 almost covered 99.3% of Shandong province. The percentage increased up to 9.2% for the area with annual mean AOD > 1.0.

Anhui was the cleanest province in the northern part of East China with only 500 km^2 area with AOD > 1.0, accounting for 0.4% of the whole district. However, the area

ACPD
11, 10485–10523, 2011

percentage with AOD > 0.5 still increased significantly from 75.3% in 2001 to 80.6% in 2007.

Among the heavy aerosol loading districts, the increment of annual mean AOD in YRD was the fastest from 2000 to 2007, where the large AOD area expand more toward north. The peak AOD is in Shanghai (especially for Baoshan district) from 2000 to 2007 in whole YRD.

3.3.2 Unbalanced variation of aerosol loading over northern and southern parts of East China

Aerosol loading over the northern part increased more than that over the southern part of East China from 2000 to 2007. The South is characterized by more cordilleras, more extensive vegetation cover and less human activities, resulting in steady aerosol loading increase, except for Poyang Lake plain with slightly deteriorated air quality. While AODs were pretty high in the North (such as the north Shanghai, Jining district in Shandong and Maanshan district in Anhui) even in the cleanest year of 2000 and 2003. Therefore, aerosol loadings in the North can be attributed definitively to anthropogenic emissions and the South to natural emissions.

3.4 Seasonal characteristics of AOD over East China

MODIS-derived AOD presented in Fig. 5 exhibits a broad range of aerosol loading in each season as well as geographical variations. In spring, the AOD maxima appeared prominently over Huaihe district and Poyang Lake plain. AOD over this area is generally higher than 0.9. Over the industrialized coastal regions of YRD, the AODs are up to 0.7. The AOD maximum in summer (up to 1.0) over YRD is caused by an increase of anthropogenic aerosols, as well as a stagnant synoptic system dominated in the Asian continent, causing building up of pollutants. The aerosol particles in summer are smaller compared with other seasons, due to the wet removals of large particles by frequent precipitations in July and August.

ACPD
11, 10485–10523, 2011

Seasonal and spatial variations of derived AOD from MODIS were related to Asian dust and anthropogenic emission patterns in spring, but modified by precipitation in summer. Regional atmospheric dispersion by strong westerly wind dominants in autumn and winter. There are large fraction of transport in spring, but relatively small amount of transport is shown in summer. The westerly wind and its strength are important in transporting dust and pollution to the downwind side of Chinese continent. The lowest AOD appeared in autumn (September–November) and winter (December–February) because aerosol loadings were strongly influenced by fast-moving synoptic weather patterns. The prevailing, strong northwesterly winds contributed to the dispersion of tropospheric aerosols. In winter, the distribution of AOD is similar to that in autumn when East China is continuously influenced by clean Asian continental air mass. The strong westerly winds in winter are similar to those in autumn. The columnar aerosol properties over East China were strongly influenced by the stationary regional meteorological conditions and the associated transport of anthropogenic aerosols from central China to the downwind regions. As a result, a huge amount of aerosols generated in coastal industrial regions worsened the air quality both local and in downwind regions. These aerosols were transported by the relatively low speed wind under stable atmospheric conditions, causing accumulations of aerosols. Formation of fine particles through gas-to-particle conversion increased due to higher solar flux in summer.

Seasonally spatial distributions in MODIS derived AOD from 2000 to 2007 showed that the AOD maximum appeared in summer over YRD, which is quite different from the conclusion by Liu et al. (2003) who used the MODIS derived AOD from 2001 to 2002 and found the AOD maximum appeared in spring. According to Duan and Mao (2007), the dust days and area under its influence decreased gradually from 2000 to 2004. Therefore, it may be considered that the Asia dust weakened over the past, and possibly led to the AOD maximum shifting from spring to summer.

ACPD
11, 10485–10523, 2011

3.5 Aerosol characteristics over typical regions in East China

Zone I, II and III with area of $100 \times 100\,km^2$ in East China were selected according to aerosol source and local meteorological condition and was shown in Fig. 7. Zone I is more frequently influenced by Asian dust, Zone II is the typical urban/industrial region, and Zone III represents the natural background with dominant continental and marine aerosol. MODIS-derived AODs are averaged in each Zone.

3.5.1 Aerosol monthly and seasonal characteristics

AOD at a particular location depends on a number of factors, including aerosol burden throughout the atmospheric column, aerosol size distributions, and its chemical composition (as it relates to the amount of water uptake and refractive index). Table 2 lists monthly and seasonal mean MODIS-derived AODs over each zone. The results clearly indicate that AOD is considerably higher during spring and summer than in winter, with minimum values in December for all zones. Monthly mean AODs in zone I and II were usually larger than 0.5, ranging from about 0.42 ± 0.25 to 0.61 ± 0.25. In zone I, AOD maximum of 1.37 ± 0.65 was found in June, and the FMFs range from 33.7 to 76.8 with maximum of 76.8 ± 28.6 in August. FMFs is lowest between November and May, when the coarse mode particles dominate in the atmosphere column. The enhanced turbidity in June was due to the formation of fine particles through gas-to-particle conversion process and the stronger turbulent that lifts aerosol particles near the surface into atmosphere.

Based on the aircraft-based, ship-based and ground-based measurements during ACE-Asia, Buzorius et al. (2004) reported the secondary aerosol formation in Asian continental outflows. They found elevated concentrations of aerosol particles in the nucleation mode, with subsequent growth in the Aitken mode from ground-based aerosol size distribution measurements. From hygroscopicity measurements, they also concluded that newly formed aerosol particles mainly consisted of ammonium sulfate. Aircraft-based measurement data showed a layer of enlarged SO_2 concentration

ACPD
11, 10485–10523, 2011

coinciding with an increased aerosol total number concentration. As additional circumstantial evidence, Yamaji et al. (2006) reported that the boundary layer O_3 concentrations in May and June were highest in the area stretching from East China to Japan. They also estimated that 30–60% of O_3 in May–June were produced by photo-chemical process through local anthropogenic emissions. Moreover, hygroscopic growth of fine hydrophilic aerosols due to the enhanced relative humidity in the lower troposphere may contribute to the peak AOD in June. Previous studies showed that the eastern Asian atmosphere has large amount of sulfate, carbon and ammonium aerosols. For example, Kim et al. (2006) showed that the hygroscopic growth of Asian aerosols was much higher than that in Europe and the eastern US. AOD experienced a decrease from 1.28 ± 0.48 to 0.77 ± 0.53 after heavy rainfall in July and August, due to the wet removal. FMFs increased to its maximum in the same period, indicating that the wet deposition by precipitation or wet removal is an important aerosol sink. Large aerosol particles are suspended in the air for a much shorter time compared with particles in accumulation mode.

In zone III, monthly mean AOD increased to its maximum in April and decreased to minimum in September. The seasonal mean AOD in this region reached maximum in spring, which was distinctly different from other regions. This seasonal variation of AOD may be a result of the dominant natural background in zone where aerosol regional transportation significantly influenced local aerosol seasonal cycle. It is interesting to note that the seasonal variation of AOD and FMF in zone III was not as large as that in the other regions, and usually larger FMF indicated that fine mode particles are dominant in the region.

ACPD
11, 10485–10523, 2011

3.5.2 Temporal variation of aerosol type

Aerosols were classified according to AOD ~ FMF method as presented in Sect. 2, and the contribution of different aerosol type was calculated as follow,

$$\tau_{m,s,c} = \frac{1}{N_{m,s}} \sum_{i=1}^{N_{m,s,c}} \tau_{i,s,c} \quad (1)$$

where $N_{m,s,c}$ is the total number of one aerosol type (s) over each zone during a given month m. $\tau_{m,s,c}$ is the monthly mean AOD of aerosol type c over zone s during month m. $N_{m,s}$ is the total number of all aerosol type over each zone during a given month. $\tau_{i,s,c}$ is an AOD sample of aerosol type c over zone s during month m.

Similarly, the frequency of each type over zone s during month m can be obtained as,

$$f_{m,s,c} = \frac{N_{m,s,c}}{N_{m,s}} \quad (2)$$

Where $f_{m,s,c}$ meets the normalization, that is

$$N_{m,s} = \sum_{c=1}^{6} N_{m,s,c} \quad (3)$$

Figure 7 shows variations of monthly mean values of $\tau_{m,s,c}$ and $f_{m,s,c}$ over the three zones from 2000 to 2007. AOD over zone (I and II) was always higher than values over zone (III). The increase of AODs over zones (I)–(III) from February to April is mainly caused by the frequent occurrence of dust. Increased anthropogenic emission may have caused the increase of AOD over those areas in June and August.

The monthly mean AOD indicated that dust contributed about 50–80% over zones (I and II), but made less than a 20% contribution over zone III. Carbonaceous aerosol types such as urban/industrial and biomass burning aerosol make up 60–80% of the

ACPD
11, 10485–10523, 2011

total AOD over zones (I and II), with 10–20% coming from biomass burning and 40–50% from urban/industrial emission. The contribution from urban/industrial aerosols increased from June to December, while the continental and marine aerosol contribution increased during the winter months, forming 20 to 40% of total aerosol loading. However, high AOD values were measured over eastern China in summer due to burning (Lee et al., 2006). Although precipitation reduces aerosol loading, increased photo chemical reaction rate combined with anthropogenic emissions are als important source terms in summer. Finally, estimates of AOD over zone (I) was much higher than those of other zones due to contributions from dust aerosols, which consisted up to 80% of the total AOD.

Figure 7 also shows that urban aerosols contributed to the high AOD values (~0.64) in zone (III) during summer, especially after 2005. Although urban pollution and biomass burning can increase AOD values in zone (III) from 2000 to 2007, continental and marine aerosols contributed too. In winter, AOD values up to 0.3 were observed in zone (III). Marine aerosol consists of up to 20–30%. The maximum contribution by continental aerosol was 50–90%. This demonstrates that continental and marine aerosols dominate thr local/regional atmospheric aerosol loading.

Atmospheric aerosols has a strong regional imbalance over the study area. In particular, the impact of anthropogenic aerosols such as urban and biomass burning aerosol was significant for local environmental conditions. This implies that anthropogenic emissions in East China can significantly modulate tropospheric aerosol radiative forcing over the study area and downwind regions.

3.6 The impact of meteorological factors to aerosol distribution and properties

3.6.1 The AOD-wind dependence

Meteorological parameters such as temperature, RH and wind greatly influence aerosol particles in their formation, scattering, aging, transport and diffusion. Aerosol properties that can be modified by these processes include size distributions, refractive index

ACPD
11, 10485–10523, 2011

and vertical distributions. Many early ground observations have demonstrated these effects (Shettle and Fenn, 1979; Horvath and Dellago, 1993).

Figure 8 presents variations of AOD and α in the three zones according to wind direction and speed. It is clear that the impact of wind on aerosol loading in different zones is closely related to local and surrounding sources, as well as terrain. Higher AOD (>1.6) and α (~1.4) can be associated with lower wind speed (<4 m s^{-1}), which indicates that the local anthropogenic emissions are dominant in Zone I. Strong southeasterly winds (~6 m s^{-1}) result in heavy aerosol loading (AOD > 1.2) due to numerous middle and small scale industries located in that area. Zone II located in YRD is characterized by urban/industrial regions with dense populations. Moderate wind regardless of wind direction brings abundant aerosol particles into this region. The easterlies brought fine urban/industrial aerosol from Shanghai downtown. Higher southeasterly wind (>6 m s^{-1}) increased AOD up to 0.8, influenced by turbidity plumes from coastal cities in Zhejiang province. Regional aerosol transportation from Anhui province can significantly increase AOD in this zone when the westerly wind prevails.

AOD in Zone III increased significantly up to 0.5 when the northwesterly wind speed reached between 3 and 6 m s^{-1}. On the other hand, easterly wind brings plenty of marine particles with larger size, reducing AOD down to 0.3 or less.

3.6.2 The RH-aerosol dependence

Figure 9 shows the scattering plots between AOD and relative humidity (RH) in the three zones. In this figure, AOD increases with RH due to hygroscopic growth of fine hydrophilic aerosols. Studies have revealed that the influence of RH on physical and chemical properties of aerosols is complex. This is primarily due to the fact that increase in RH can enhance particle growth through condensation, coagulation and resuspension. This leads to the increase in light scattering, either due to increase in particle sizes and/or increase in the particle number density. In this study, we adopted the Kasten–Hanel experiential formula to investigate the dependence of AOD on RH as follow,

ACPD
11, 10485–10523, 2011

$$\sigma = \sigma_0(1 - \mathrm{RH})^{-\gamma} \quad (4)$$

Where σ and $\sigma 0$ are the scattering coefficients corresponding to RH and dry condition, respectively. γ is the hygroscopic growth coefficient.

Regardless of the aerosol absorption and the discrepancy of aerosol hygroscopic growth in different height, Eq. (4) can be transformed as,

$$\tau = \tau_0(1 - \mathrm{RH})^{-\gamma} \quad (5)$$

The dependence of AOD on RH in the three zones was fitted according to Eq. (5) and the fitted curves were plotted in Fig. 9. The hygroscopic growth coefficients γ are 1.3965, 0.615 and 0.3341; the slopes of fitted curves are 0.0234, 0.0135 and 0.0047; the correlation coefficients are 0.5495, 0.4401 and 0.3176 in zones (I–III) respectively. It is remarkable that the slope and γ in zone I are higher than those in the other zones, indicating more obvious hygroscopic growth and more sensitive aerosol properties on RH. One possible reason is that aerosols in zone III, located in Southeast China with higher RH, tend to saturate in hygroscopic growth effect. On the other hand, aerosol size in zone I usually represents more remarkable growth under the condition of extensive RH variation.

Plenty of urban/industrial aerosols suspended over zones I and II. Urban/industrial aerosol model which represents strong pollution in urban areas includes insoluble, water soluble and soot aerosol species (Hess et al., 1998). The insoluble aerosols are mostly soil particles with certain amount of organic material. The water soluble component that originated from gas to particle conversion contains various kinds of sulfate, nitrate, and other organics. Urban/industrial aerosol model has 28 000 water soluble particles per cm^3, 1.5 insoluble particles and 130 000 soot particles (Hess et al., 1998). In Table 3, the physical (mode radius and density) and optical (aerosol optical depth) properties of water soluble aerosol components for urban/industrial aerosol model as a function of relative humidity are given. The 550 nm AOD for urban/industrial aerosol model increases more than 3 folds when RH increases from 0% to 95%.

ACPD
11, 10485–10523, 2011

3.6.3 AOD-temperature dependence

Correlation coefficient of AOD-T in the three zones was calculated according to different seasons. The result showed that the correlation coefficient of AOD-T for all samples in zone I is 0.3475, but it increases up to 0.5279 for winter, which is much higher than other zones.

Figure 10 shows the variation of AOD with temperature confined by season and wind condition. "•" represents conditions where wind speed is less than 8 m s^{-1} and wind direction is between 60 and 90, where the correlation coefficient of AOD-T was 0.6663. "∘" represents conditions with wind speed of 4–5 m s^{-1} and wind direction between 190 and 220, where the correlation coefficient of AOD-T was 0.8913. "Δ" represents codi-tions with wind speed of 1–3 m s^{-1} and wind direction between 190 and 240, where the correlation coefficient of AOD-T was 0.7875. "□" represents conditions where wind speed is less than 1 m s^{-1} and wind direction is between 190 and 300, where the correlation coefficient of AOD-t was 0.9236. "+" represents conditions where wind speed is less than 5 m s^{-1} and wind direction is between 200 and 290, where the correlation coefficient of AOD-t was 0.6941. "∗" represents conditions with wind speed of 1–5 m s^{-1} and wind direction between 300 and 360, where the correlation coefficient of AOD-t was 0.9473. In Fig. 10d, "•" and "+" are the comparison of AOD and α versus temperature at wind speed less than 5 m s^{-1} and wind direction between 100 and 200, and the solid and dashed line are the fitted line for AOD and α, the correlation coefficient of AOD-T and α-T are 0.6514 and 0.5639, the slopes of fitted lines are 0.0323 and 0.01956, respectively. These comparisons indicate that AOD and α usually increase with the enhanced temperature, which is related to the atmospheric photochemical effect such as gas-particle conversion process. The increasing temperature accompanied by enhanced solar radiation is in favor of gas-particle conversion process and produces more fine mode particles. Furthermore, aerosols from different sources have different photochemical processes because of their different chemical components.

ACPD
11, 10485–10523, 2011

4 Conclusion

We present results of aerosol spatial distributions, seasonal and inter-annual variabilities, and the influence of meteorological conditions on aerosol physical properties derived from MODIS over East China from 2000 to 2007. Four high AOD values are found in northwest plain in Shandong province, Huanghuai, Poyang Lake Plain and the Yangtze River Delta region (particularly the vicinity around the Yangtze River), with relative abundant coarse mode particles in the atmospheric column.

The dominant aerosols in the southern part of East China (excluding the Poyang Lake plain) are continental, marine and mixed types. The dominant continental aerosol type was observed in southern Anhui and central Zhejiang. Abundant marine aerosols were found over the mountain area of southwest. We also found that the dominant aerosol type over coastal zone is mixed aerosol rather than marine aerosol. This is possibly because of some small cities where relatively frequent human activities produce plenty of anthropogenic pollutants. The dominant aerosols over YRD are soil dust and urban/industrial pollutants. AODs show an increasing trend during the eight-year period, and the zone with AOD > 0.5 and AOD > 1.0 have been expanding year by year, especially after 2005. Of the high aerosol loading districts, the increase of annual mean AOD in YRD was fastest from 2000 to 2007, where large AOD extends more to the northward than southward. The peak AOD occurred in Shanghai (especially for Baoshan district) from 2000 to 2007 in the whole YRD. Moreover, aerosol loading over the northern part increased more obviously than that over the southern part of East China. In spring, the AOD maxima appeared over Huaihe district and Poyang Lake plain. Maximum AOD in summer (up to 1.0) over YRD is caused by an increase of anthropogenic aerosols as well as a stagnant synoptic meteorological system dominant in Asian continent, causing a build-up of pollutants in this region. Seasonal variations of derived MODIS AOD from 2000 to 2007 showed that the AOD maximum appeared in summer over YRD, which is quite different from a previous study by Liu et al. (2003). They found that the AOD maximum appeared in spring using the derived MODIS AOD

ACPD
11, 10485–10523, 2011

from 2001 to 2002. The reason may be that Asian dust weakened, possibly leading to the maximum AOD shifting from spring to summer.

Three zones with area of $100 \times 100\,km^2$ in East China were selected according to aerosol source and local meteorological condition. Dust contributed about 50–80% to the monthly mean AOD over zones (I and II), but less than 20% cover zone III. Carbonaceous aerosol type shows a strong summer peak, contributing up to 60–80% of the total AOD over zones (I and II). In zone (III), continental and marine aerosols make relatively high contributions to the local/regional atmospheric aerosol loading. Meteorological parameters such as temperature, RH and wind can greatly influence aerosol loadings, with different effects on different aerosol sources.

Acknowledgements. The study is partially supported by the research grants from the National Natural Science Foundation of China (NSFC, Grant Numbers: 40705013, 40575001 and 40775002), the National High Technology Research and Development Program of China (863 Major Project, No. 2006AA06A303), the Shanghai Science and Technology Committee Research Special Funds (Grant Number: 10JC1401600, 10231203803 and 10231203900) and the China Meteorological Bureau Public Welfare Special Funds (Grant Number: GYHY(QX)200706019). The authors gratefully acknowledge the MODIS Science Data Support Team and the Earth Observing System Data Gateway for processing and distributing MODIS data used in this paper, respectively. We would like to thank the three anonymous reviewers, whose useful comments have improved the paper.

References

Barnaba, F. and Gobbi, G. P.: Aerosol seasonal variability over the Mediterranean region and relative impact of maritime, continental and Saharan dust particles over the basin from MODIS data in the year 2001, Atmos. Chem. Phys., 4, 2367–2391, doi:10.5194/acp-4-2367-2004, 2004.

Buzorius, G., McNaughton, C. S., Clarke, A. D., Covert, D. S., Blomquist, B., Nielsen, K., and Brechtel, F. J.: Secondary aerosol formation in continental outflow conditions during ACE-Asia, J. Geophys. Res., 109, D24203, doi:10.1029/2004JD004749, 2004.

Charlson, R. J., Schwartz, S. E., Hales, J. M., Cess, R. D., Coakley, J. A., Hansen, J. E., and Hofmann, D. J.: Climate forcing by anthropogenic aerosols, Science, 255, 423–430, 1992.
Chu, D. A., Kaufman, Y. J., Zibordi, G., Chern, J. D., Mao, J., Li, C., and Holben, B. N.: Global monitoring of air pollution over land from the Earth Observing System-Terra Moderate Resolution Imaging Spectroradiometer (MODIS), J. Geophys. Res., 108, 4661, doi:10.1029/2002JD003179, 2003.
Chu, D. A., Remer, L. A., Kaufman, Y. J., Schmid, B., Redemann, J., Knobelspiesse, K., Chern, J. D., Livingston, J., Russell, P. B., Xiong, X., and Ridgway, W.: Evaluation of aerosol properties over ocean from Moderate Resolution Imaging Spectroradiometer (MODIS) during ACE-Asia, J. Geophys. Res., 110, D07308, doi:10.1029/2004JD005208, 2005.
Climate Change 2001: The Scientific Basis, Contribution of Working Group I to the Third Assessment Report of the Intergovernmental Panel on Climate Change, edited by: Houghton, J. T., Ding, Y., Griggs, D. J., Noguer, M., Van der Linden, P. J., Dai, X., Maskell, K., and Johnson, C. A., Cambridge Univ. Press, New York, 349–416, 2001.
Duan, J. and Mao, J. T.: Study on the distribution and variation trends of atmospheric aerosol op tical dep th over the Yangtze River Delta, Acta Scientiae Circumstantiae, 27(4), 537–543, 2007.
Dubovik, O., Holben, B. N., Eck, T. F., Smirnov, A., Kaufman, Y. J., King, M. D., Tanre, D., and Slutsker, I.: Variability of absorption and optical properties of key aerosol types observed in worldwide locations, J. Atmos. Sci., 59, 590–608, 2002.
Haywood, J. M. and Boucher, O: Estimates of the direct and indirect radiative forcing due to tropospheric aerosol: A review, Rev. Geophys., 38, 513–543, 2000.
He, Q. S., Li, C. C., Mao, J. T., Lau, A. K. H., and Li, P. R.: A study on the aerosol extinction-to-backscatter ratio with combination of micro-pulse LIDAR and MODIS over Hong Kong, Atmos. Chem. Phys., 6, 3243–3256, doi:10.5194/acp-6-3243-2006, 2006.
Hess, M., Koepke, P., and Schult, I.: Optical properties of aerosols and clouds: The software package OPAC, Bull. Am. Meteorol. Soc., 79, 831–844, 1998.
Huebert, B. J., Bates, T., Russell, P. B., Shi, G., Kim, Y. J., Kawamura, K., Carmichael, G., and Nakajima, T.: An overview of ACE-Asia: Strategies for quantifying the relationships between Asian aerosols and their climatic impacts, J. Geophys. Res., 108(D23), 8633, doi:10.1029/2003JD003550, 2003.

ACPD
11, 10485–10523, 2011

Hutchison, K. D., Smith, S., and Faruqui, S. J.: Correlating MODIS aerosol optical thickness data with ground-based PM2.5 observations across Texas for use in a real-time air quality prediction system, Atmos. Environ., 39, 7190–7203, 2005.

Horvath, H. and Dellago, C.: On the accuracy of the size distribution information obtained from light extinction and scattering measurements: II. Case studies, J. Aerosol Sci., 24, 143–154, 1993.

Kaufman, Y. J., Tanré, D. L., Remer, A., Vermote, E. F., Chu, A., and Holben, B. N.: Operational remote sensing of tropospheric aerosol over land from EOS moderate resolution imaging spectroradiometer, J. Geophys. Res., 102, 17051–17067, 1997.

Kaufman, Y. J., Tanre, D., Leon, J. F., and Pelon, J.: Retrievals of profiles of fine and coarse aerosols using lidar and radiometric space measurements, IEEE T. Geosci. Remote, 41, 1743–1754, 2003.

Kim, D. H., Sohn, B. J., Nakajima, T., and Takamura, T.: Aerosol radiative forcing over east Asia determined from ground-based solar radiation measurements, J. Geophys. Res., 110, D10S22, doi:10.1029/2004JD004678, 2005.

Kim, S. W., Yoon, S. C., Jefferson, A., Ogren, J. A., Dutton, E. G., Won, J. G., Ghim, Y. S., Lee, B. I., and Han, J. S.: Aerosol optical, chemical, and physical properties at Gosan, Korea during Asian dust and pollution episodes in 2001, Atmos. Environ., 39(1), 39–50, 2005

Kim, J., Yoon, S.-C., Jefferson, A., and Kim, S.-W.: Aerosol hygroscopic properties during Asian dust, pollution, and biomass burning episodes at Gosan, Korea in April 2001, Atmos. Environ., 40(8), 1550–1560, 2006.

King, M. D., Kaufman, Y. J., Menzel, W. P., and Tanre, D.: Remote sensing of cloud, aerosol, and water vapor properties from the Moderate Resolution Imaging Spectrometer (MODIS), IEEE T. Geosci. Remote, 30, 2–27, 1992.

Levine, J. S., Cofer, W. R., Cahoon, D. R., and Winstead, E. L.: Biomass burning: A driver for global change, Environ. Sci. Technol., 29(3), 120–125, 1995.

Levy, R. C., Remer, L. A., Tanre, D., Kaufman, Y. J., Ichoku, C., Holben, B. N., Livingston, J. M., Russell, P. B., and Maring, H.: Evaluation of the Moderate-Resolution Imaging Spectroradiometer (MODIS) retrievals of dust aerosol over the ocean during PRIDE, J. Geophys. Res., 108(D19), 8594, doi:10.1029/2002JD002460, 2003.

Levy, R. C., Remer, L. A., Mattoo, S., Vermote, E. F., and Kaufman, Y. J.: Second-generation operational algorithm: Retrieval of aerosol properties over land from inversion of Moderate Resolution Imaging Spectroradiometer spectral reflectance, J. Geophys. Res., 112, D13211,

ACPD
11, 10485–10523, 2011

doi:10.1029/2006JD007811, 2007.
Li, Z.: Aerosol and climate: A perspective from East Asia, in Observation, Theory, and Modeling of the Atmospheric Variability, 501–525, World Sci., Hackensack, N. J., 2004.
Luo, Y. F., Lu, D. R., Zhou, X. J., Li, W. L., and He, Q.: Characteristics of the spatial distribution and yearly variation of aerosol optical depth over China in last 30 years, J. Geophys. Res., 106, 14501–14513, 2001
Mao, J. T. and Li., C. C.: Observation study of aerosol radiative properties over china, Acta Meteorol. Sin., 63(5), 622–635, 2005.
Menon, S., Hansen, J. E., Nazarenko, L., and Luo, Y. F.: Climate effects of black carbon aerosols in China and India, Science, 297, 2249–2252, 2002.
Nakajima, T., Sekiguchi, M., Takemura, T., Uno, I., Higurashi, A., Kim, D., Sohn, B. J., Oh, S. N., Nakajima, T. Y., Ohta, S., Okada, I., and Takamura, T.: Significance of direct and indirect radiative forcings of aerosols in the East China Sea region, J. Geophys. Res., 108(D23), 8658, doi:10.1029/2002JD003261, 2003.
Lee, K. H., Kim, Y. J., and Han, J. S.: Characteristics of aerosol observed during two severe haze events over Korea in June and October 2004, Atmos. Environ., 40(27), 5146–5155, 2006.
Liu, G. Q., Li, C. C., Zhu, A. H., and Mao, J. T.: Optical depth research of atmospheric aerosol in the Yangtze River Delta region, Shanghai Environ. Sci., appl., 58–63, 2003.
Pilinis, C., Pandis, S. N., and Seinfeld, J. H.: Sensitivity of direct climate forcing by atmospheric aerosols to aerosol size and composition, J. Geophys. Res., 100(D9), 18739–18754, 1995.
Qian, Y. and Giorgi, F: Regional climatic effects of anthropogenic aerosols? The case of south-western China, Geophys. Res. Lett., 27, 3521–3524, 2000.
Ramachandran, S.: Aerosol optical depth and fine mode fraction variations deduced from Moderate Resolution Imaging Spectroradiometer (MODIS) over four urban areas in India, J. Geophys. Res., 112, D16207, doi:10.1029/2007JD008500, 2007.
Remer, L. A. and Kaufman, Y. J.: Dynamic aerosol model: Urban/industrial aerosol, J. Geophys. Res., 103, 13859–13871, 1998.
Remer, L. A., Kaufman, Y. J., Tanre, D., Mattoo, S., Chu, D. A., Martins, J. V., Li, R., Ichoku, C., Levy, R. C., and Kleidman, R. G.: The MODIS aerosol algorithm, products, and validation, J. Atmos. Sci., 62(4), 947–973, 2005.

ACPD
11, 10485–10523, 2011

Shettle, E. P. and Fenn, R. W.: Models for the aerosols of the lower atmosphere and the effects of humidity variations on their optical properties, AFGL-TR-79-0214, 94 pp., Air Force Geophys. Lab., Hanscom Air Force Base, Mass, 1979.

Tang, J., Xue, Y., Yu, T., and Guan, Y.: Aerosol optical thickness determination by exploiting the synergy of TERRA and AQUA MODIS, Remote Sens. Environ., 94, 327–334, 2005.

Yamaji, K., Ohara, T., Uno, I., Tanimoto, H., Kurokawa, J., and Akimoto, H.: Analysis of the seasonal variation of ozone in the boundary 30 layer in east Asia using the community multi-scale air quality model: what controls surface ozone levels over Japan?, Atmos. Environ., 40(9), 1856–1868, 2006.

Xu, Q.: Abrupt change of the midsummer climate in central east China by the influence of atmospheric pollution, Atmos. Environ., 35, 5029–5040, 2001.

Xu, J., Bergin, M. H., Yu, X., Liu, G., Zhao, J., Carrico, C. M., and Baumann, K.: Measurement of aerosol chemical, physical and radiative properties in the Yangtze delta region of China, Atmos. Environ., 36(2), 161–173, 2002.

ACPD
11, 10485–10523, 2011

Table 1. The annual mean aerosol-related parameters in three key districts of East China.

YRD									
Year	[a]$S_{0.5}$	$S_{1.0}$	[b]$P_{0.5}$	$P_{1.0}$	[c]τ_{max}	τ_{min}	τ_{mean}	[d]L_{max}	L_{min}
2000	1.005	0.003	60.1	0.2	1.07	0.16	0.57	121.8 31.2	119.2 27.5
2001	1.079	0.000	61.8	0.0	0.98	0.17	0.56	119.3 32.8	119.1 27.8
2002	1.091	0.008	62.1	0.5	1.73	0.14	0.60	120.5 33.8	119.1 27.7
2003	1.067	0.003	60.9	0.2	1.11	0.18	0.58	122.0 31.0	120.9 33.0
2004	1.075	0.007	61.4	0.4	1.18	0.18	0.58	121.9 31.1	122.0 31.8
2005	1.124	0.003	62.8	0.2	1.16	0.22	0.60	120.0 31.2	119.1 27.8
2006	1.159	0.041	65.9	2.3	1.61	0.21	0.65	120.2 31.3	118.8 28.2
2007	1.174	0.076	66.6	4.3	2.37	0.20	0.68	118.6 33.2	119.1 27.7
All	1.132	0.003	63.2	0.2	1.13	0.20	0.61	120.0 31.2	119.1 27.8
Shandong									
Year	$S_{0.5}$	$S_{1.0}$	$P_{0.5}$	$P_{1.0}$	τ_{max}	τ_{min}	τ_{mean}	L_{max}	L_{min}
2000	1.145	0.000	74.8	0.0	0.95	0.16	0.59	118.7 37.4	122.4 37.4
2001	1.072	0.000	70.0	0.0	0.97	0.10	0.58	116.3 35.1	121.1 37.7
2002	1.326	0.007	86.6	0.5	1.98	0.28	0.64	119.5 37.1	122.6 37.2
2003	1.521	0.025	99.3	1.6	1.66	0.28	0.76	121.4 37.5	118.9 37.5
2004	1.205	0.001	78.7	0.07	1.01	0.23	0.61	118.9 37.2	122.6 37.2
2005	1.510	0.007	98.2	0.5	1.09	0.44	0.73	118.7 37.3	117.2 36.4
2006	1.521	0.141	99.3	9.2	1.74	0.44	0.81	119.2 37.1	118.2 36.3
2007	1.497	0.051	98.0	3.3	1.78	0.36	0.75	119.1 37.1	118.7 38.1
All	1.462	0.001	95.1	0.07	1.00	0.42	0.69	118.7 37.4	120.9 37.2
Anhui									
Year	$S_{0.5}$	$S_{1.0}$	$P_{0.5}$	$P_{1.0}$	τ_{max}	τ_{min}	τ_{mean}	L_{max}	L_{min}
2000	1.016	0.000	75.8	0.0	0.98	0.23	0.62	117.3 31.6	116.2 31.1
2001	1.010	0.000	75.3	0.0	0.89	0.21	0.59	118.3 31.6	118.8 30.1
2002	1.022	0.000	76.2	0.0	0.98	0.22	0.61	119.2 32.8	116.1 31.0
2003	1.045	0.000	77.9	0.0	0.98	0.23	0.64	116.9 32.2	116.1 31.0
2004	1.040	0.000	77.6	0.0	0.91	0.25	0.61	116.3 29.9	116.1 31.1
2005	1.040	0.000	77.6	0.0	0.92	0.26	0.64	116.4 30.0	118.8 30.1
2006	1.037	0.000	77.3	0.0	0.97	0.26	0.64	117.2 31.8	116.2 31.0
2007	1.081	0.005	80.6	0.4	1.14	0.26	0.70	117.6 31.5	116.2 31.0
All	1.037	0.000	77.3	0.0	0.91	0.26	0.63	117.2 31.8	118.8 30.1

[a] $S_{0.5}$ represents the area with $\tau > 0.5$. The same as $S_{1.0}$ but for $\tau > 1.0$. Unit: 10^5 km^2.
[b] $P_{0.5}$ represents the proportion of area where the AOD > 0.5 to the different regions. The same as $P_{1.0}$ but for $\tau > 1.0$.
[c] τ_{max}, τ_{min} and τ_{mean} are the maximum, minimum and mean AOD in the study region respectively.
[d] L_{max} and L_{min} are the location (longitude ° E latitude ° N) of maximum and minimum mean AOD in the study region respectively.

ACPD
11, 10485–10523, 2011

Table 2. The monthly and seasonal mean AOD and FMF in the three zones from the MODIS L2 product between 2000 and 2007. The numbers in the parentheses are the standard bias.

Region	I		II		III	
Month	AOD	fmf	AOD	fmf	AOD	fmf
Jan	0.47(0.26)	19.4(34.1)	0.62(0.23)	32.3(42.8)	0.32(0.19)	58.1(33.3)
Feb	0.60(0.39)	8.7(22.2)	0.73(0.31)	15.8(29.9)	0.36(0.19)	64.0(29.9)
Mar	0.83(0.49)	13.7(26.4)	0.90(0.39)	21.0(33.4)	0.48(0.29)	51.5(34.3)
Apr	1.05(0.58)	17.9(28.0)	1.03(0.37)	23.4(33.6)	0.51(0.28)	52.0(37.4)
May	1.12(0.68)	19.8(29.3)	1.08(0.44)	23.6(31.8)	0.44(0.22)	65.6(34.5)
Jun	1.37(0.65)	33.7(34.5)	1.28(0.48)	42.2(34.3)	0.47(0.32)	81.5(26.0)
Jul	1.26(0.96)	72.4(31.5)	0.98(0.54)	65.9(34.2)	0.35(0.23)	81.0(28.8)
Aug	0.87(0.69)	76.8(28.6)	0.77(0.53)	70.3(30.2)	0.40(0.25)	84.9(26.0)
Sep	0.77(0.65)	55.8(33.3)	0.72(0.39)	53.2(35.1)	0.35(0.23)	90.7(16.6)
Oct	0.71(0.56)	28.7(35.3)	0.70(0.34)	19.0(31.0)	0.34(0.22)	79.3(26.0)
Nov	0.51(0.32)	14.4(27.4)	0.67(0.28)	16.2(28.4)	0.30(0.24)	67.4(30.8)
Dec	0.42(0.25)	12.8(27.2)	0.61(0.25)	19.2(32.1)	0.25(0.21)	65.8(32.0)
Spring	1.01(0.61)	17.4(28.1)	1.01(0.41)	22.7(32.9)	0.48(0.27)	56.2(36.0)
Summer	1.17(0.81)	60.7(37.2)	0.99(0.56)	61.2(34.8)	0.39(0.26)	82.4(27.3)
Autumn	0.67(0.54)	33.3(36.5)	0.70(0.34)	28.6(35.5)	0.33(0.23)	79.1(26.8)
Winter	0.49(0.31)	13.5(28.4)	0.66(0.27)	21.5(35.1)	0.30(0.20)	62.8(31.9)

ACPD
11, 10485–10523, 2011

Table 3. Physical (Mode Radius, rm, and Density, r, of Water Soluble Aerosol Component) and Optical (Aerosol Optical Depth (AOD) at 550 nm) Properties for Urban Aerosol Model (Hess et al., 1998) as a Function of Relative Humidity (RH) Varying From 0 to 95%.

RH %	r_mµm	ρ g cm^{-3}	τ (550 nm)
0	0.0212	1.80	0.362
50	0.0262	1.42	0.484
70	0.0285	1.33	0.560
80	0.0306	1.27	0.643
90	0.0348	1.18	0.849
95	0.0399	1.12	1.178

ACPD
11, 10485–10523, 2011

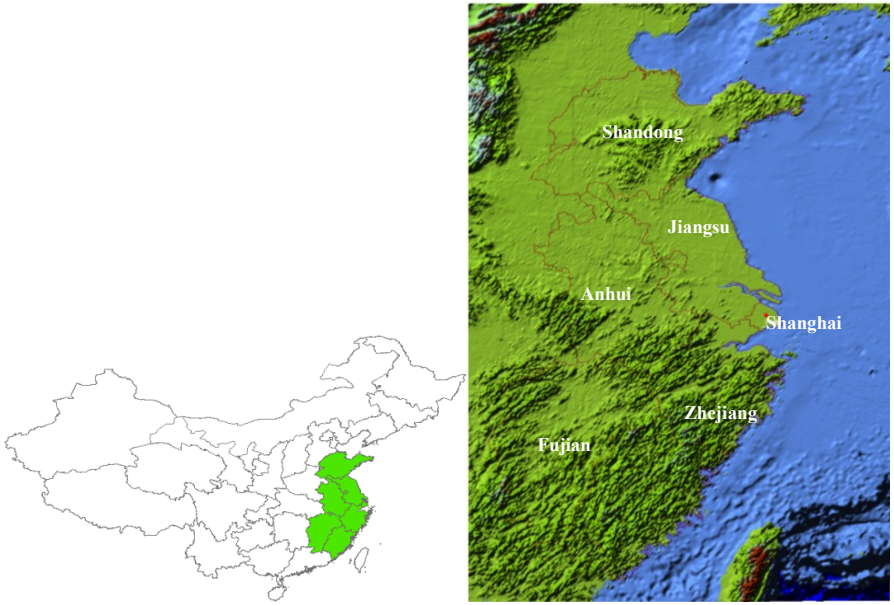

Fig. 1. The location and terrain of East China.

ACPD
11, 10485–10523, 2011

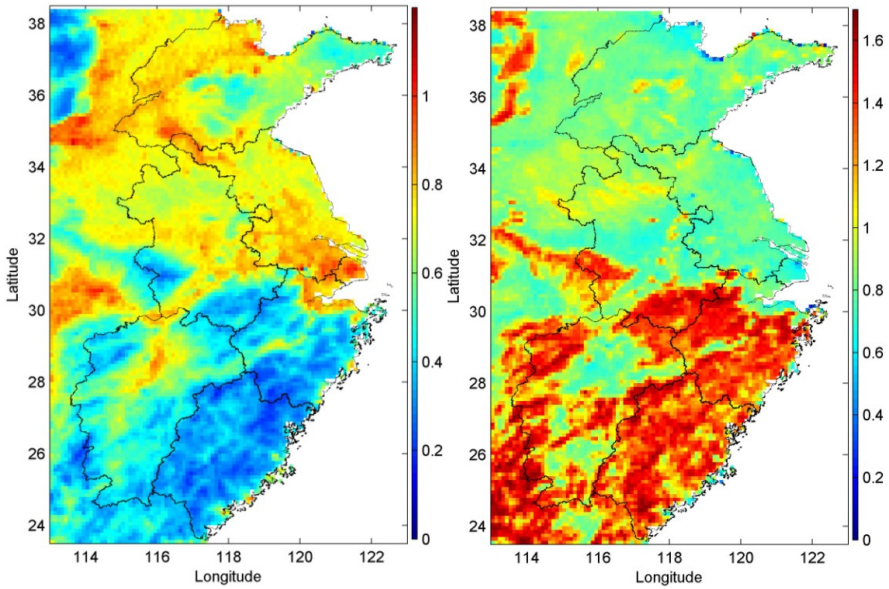

Fig. 2. The distribution of **(a)** AOD and **(b)** α over East China averaged from MODIS level 2 product in the period of 2000–2007.

ACPD
11, 10485–10523, 2011

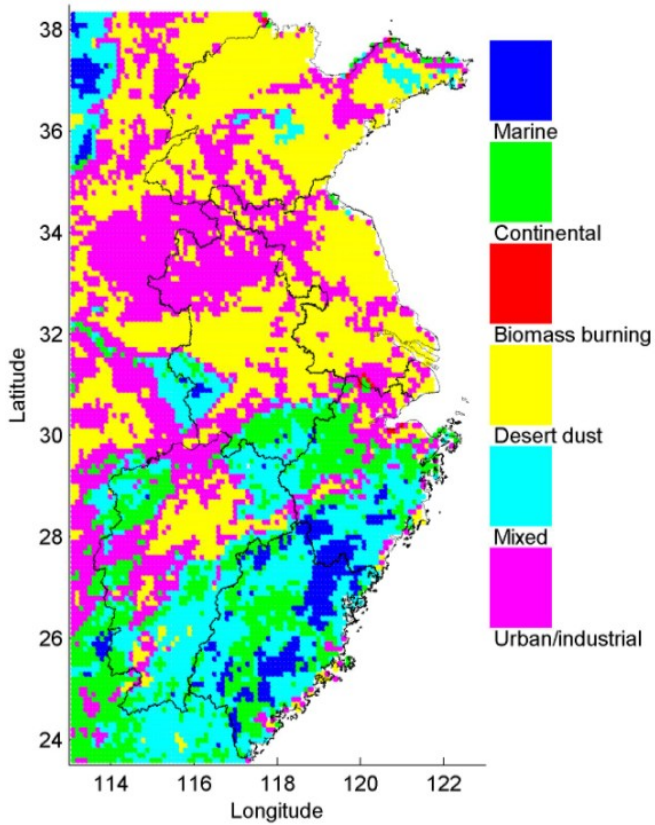

Fig. 3. The aerosol type distribution in East China according to the AOD ~ FMF classification method based on the MODIS product from 2000 to 2007.

ACPD
11, 10485–10523, 2011

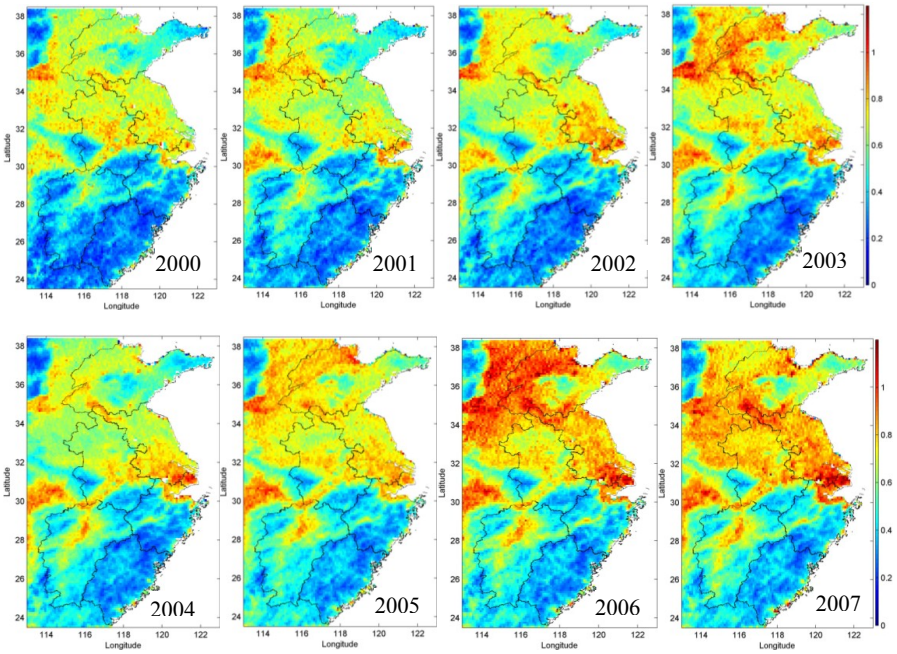

Fig. 4. The distribution of annual mean AOD over East China for 2000–2007.

ACPD
11, 10485–10523, 2011

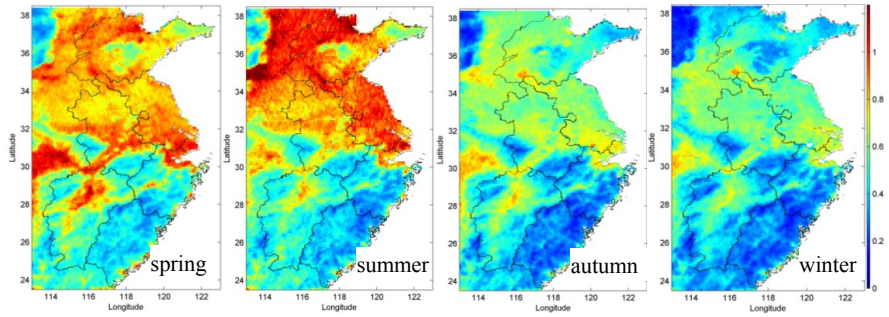

Fig. 5. The distribution of seasonal mean AOD over East China from the MODIS L2 product between 2000 and 2007.

ACPD
11, 10485–10523, 2011

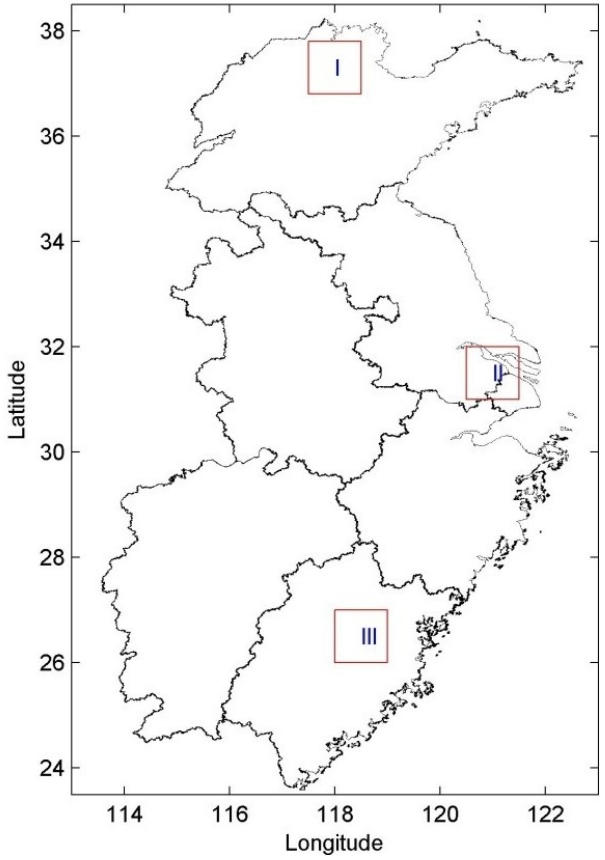

Fig. 6. The location of three typical zones with each area of $100 \times 100\,km^2$ in East China according to their aerosol source and local meteorological condition. The Roman numbers in the frame are the name of the zones.

ACPD
11, 10485–10523, 2011

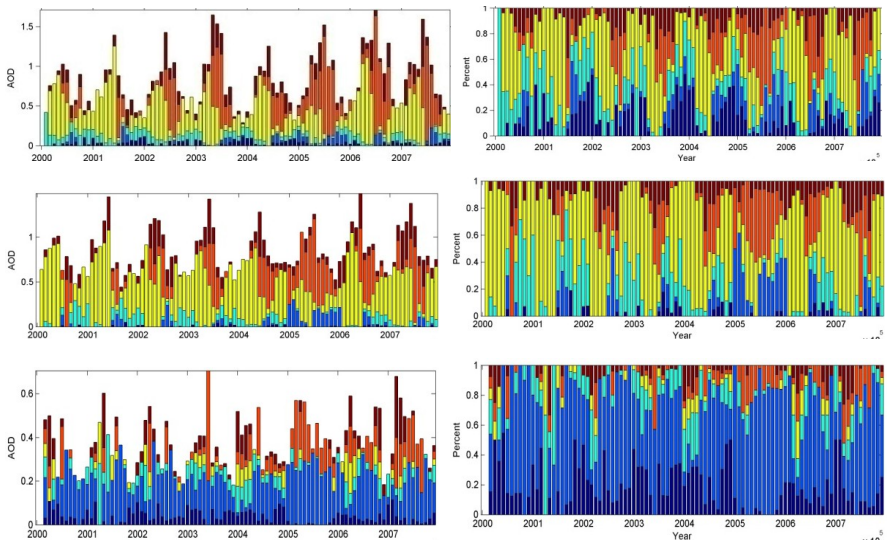

Fig. 7. (a–c) The temporal variation of monthly mean MODIS-derived AOD in the three zones from 2000 to 2007. The color, same as Fig. 3, is the proportion of specific aerosol type in total AOD. **(d–f)** The temporal variation of normalized frequency for specific aerosol type in the three zones from 2000 to 2007.

ACPD
11, 10485–10523, 2011

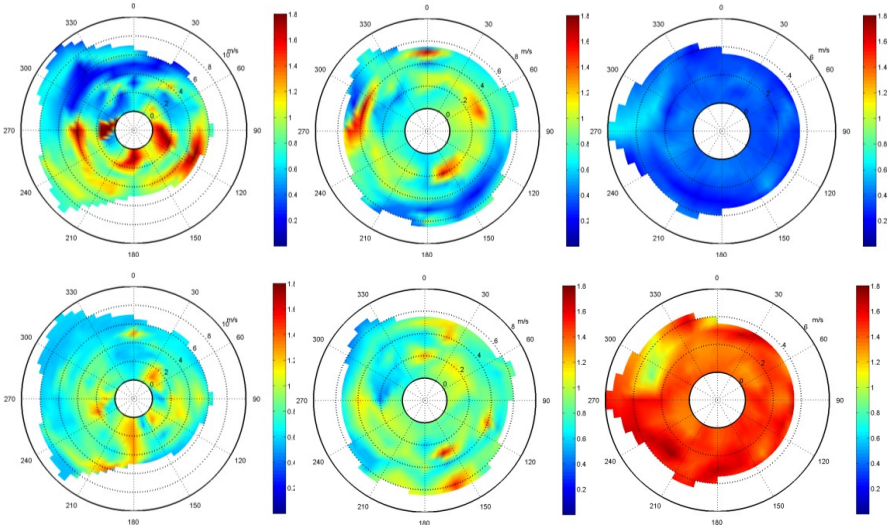

Fig. 8. The variation of AOD (up panel) and α (down panel)in zone **(a)** I, **(b)** II and **(c)** III according to the wind direction and wind speed.

ACPD
11, 10485–10523, 2011

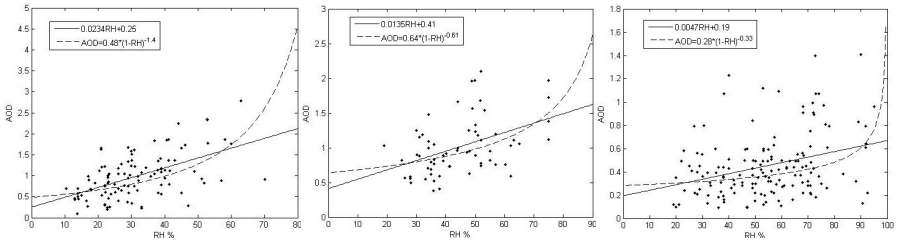

Fig. 9. The scattering dots between AOD and RH in spring over zone **(a)** I, **(b)** II and **(c)** III. The curve and line are the fitted results based on Eq. (5) and linearity, respectively.

ACPD
11, 10485–10523, 2011

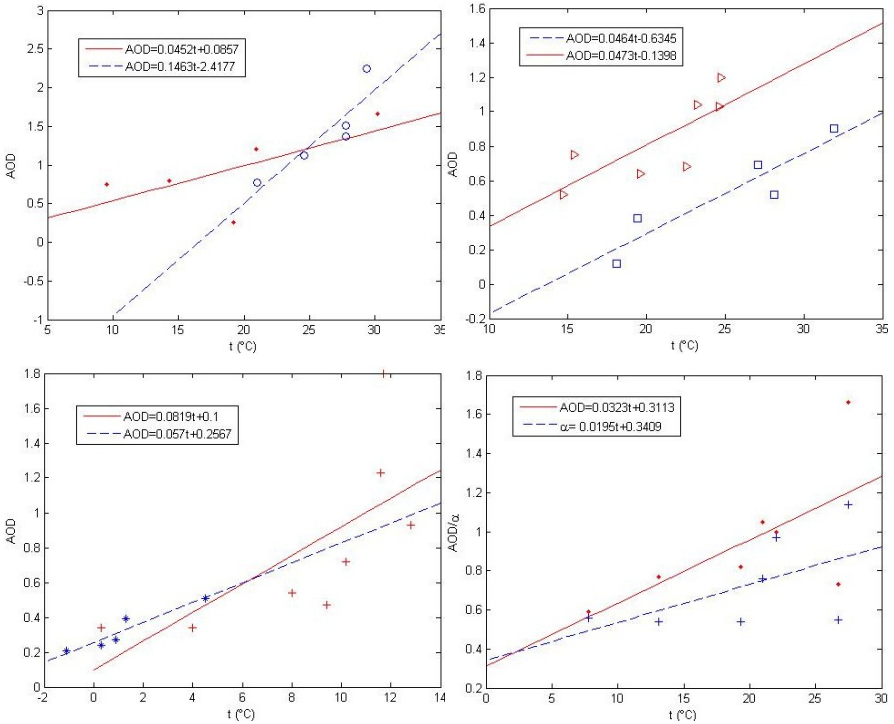

Fig. 10. The scattering dots between AOD and temperature in zone I for **(a)** spring, **(b)** autumn and **(c)** winter. **(d)** The scattering dots between AOD/α and temperature in zone II for spring. The curves are the fitted lines.

ACPD
11, 10485–10523, 2011